The results presented above were obtained by assuming an incident δ-source. For the derivation of the solution of a finite flat beam incident onto the center of the cylinder top we use the diffusion equation for the rotationally symmetric case (no ϕ-dependence)

$$\frac{\partial^2}{\partial\rho^2}\Phi+\frac{1}{\rho}\frac{\partial}{\partial\rho}\Phi+\frac{\partial^2}{\partial z^2}\Phi-\left(\frac{\mu_a}{D}+i\frac{\omega}{Dc}\right)\Phi=-\frac{1}{D}S(\vec{r},\omega)\,, \tag{25}$$

where $S(\vec{r},\omega)$ is a rotationally symmetric source. For a flat beam we have

$$S(\vec{r},\omega)=\frac{1}{\pi\rho_w^2}\mathrm{circ}\left(\frac{\rho}{\rho_w}\right)\delta(z-z_0)\,, \tag{26}$$

where ρ_w is the radius of the flat beam and circ is defined as

$$\mathrm{circ}\left(\frac{\rho}{\rho_w}\right)=\begin{cases}1, & \rho\le\rho_w\\ 0, & \rho>\rho_w\end{cases}\,. \tag{27}$$

By employing the finite Hankel transform of zero order, Eq. (25) becomes

$$\frac{\partial^2}{\partial z^2}\Phi-\left(\frac{\mu_a}{D}+s_n^2+i\frac{\omega}{Dc}\right)\Phi=-\frac{1}{D}S(s_n,z,\omega)=-\frac{1}{D}\frac{J_1(s_n\rho_w)}{\pi s_n\rho_w}\delta(z-z_0)\,. \tag{28}$$

By using the solution of Eq. (9), $G(s_n,z,\omega)$, Eq. (28) is solved with

$$\Phi(s_n,z,\omega)=\frac{J_1(s_n\rho_w)}{\pi s_n\rho_w}G(s_n,z,\omega)\,. \tag{29}$$

The inverse relation for the finite Hankel transform of zero order is

$$\Phi(\vec{r},\omega)=\frac{2}{a'^2}\sum_{n=1}^{\infty}\Phi(s_n,z,\omega)J_0(s_n\rho)J_1^{-2}(s_na')\,. \tag{30}$$

Thus, the solution of the diffusion equation for an incident flat beam is given by

$$\Phi(\vec{r},\omega)=\frac{2}{\pi a'^2\rho_w}\sum_{n=1}^{\infty}G(s_n,z,\omega)\frac{J_0(s_n\rho)J_1(s_n\rho_w)}{s_nJ_1^2(s_na')}\,. \tag{31}$$

We note that Eq. (31) is also used for solving the diffusion equation for N-layered turbid media, see the accompanying paper [10]. The final step for obtaining the complete solutions is the derivation of the Green's function, G, see Eq. (9). The boundary conditions in z-direction for the homogeneous cylinder are given by

$$\begin{aligned}&\Phi(\rho,\phi,z=-z_b,\omega)=0\\ &\Phi(\rho,\phi,z=l_z+z_b,\omega)=0\,.\end{aligned} \tag{32}$$

Below we present two solutions in the frequency and two solutions in the time domains.

Solutions in the frequency domain

Version A

We start with the ordinary differential equation given in Eq. (9). It can be solved with the method of image sources where the exponential functions are summed to satisfy the boundary conditions for the z-direction given in Eq. (32). The solution is

$$G(s_n,z,\omega)=\frac{1}{2D\alpha}\sum_{k=-\infty}^{\infty}\exp\left(-\alpha\left|z-z_{1k}\right|\right)-\exp\left(-\alpha\left|z-z_{2k}\right|\right)\,, \tag{33}$$

where

$$\begin{aligned} z_{1k} &= 2kl_z + 4kz_b + z_0 \\ z_{2k} &= 2kl_z + (4k-2)z_b - z_0 \\ \alpha &= \sqrt{\frac{\mu_a}{D} + s_n^2 + i\frac{\omega}{Dc}}\,. \end{aligned} \tag{34}$$

Thus, by inserting Eq. (33) in Eq. (20) we obtain the fluence rate for the pencil beam incident at an arbitrary location onto the cylinder as

$$\begin{aligned} \Phi(\vec{r},\omega) &= \frac{1}{2\pi D a'^2}\sum_{m=-\infty}^{\infty}\cos(m\varphi)\sum_{n=1}^{\infty}\frac{J_m(s_n\rho_0)J_m(s_n\rho)}{\alpha J_{m+1}^2(a's_n)} \\ &\quad\times\sum_{k=-\infty}^{\infty}\exp\left(-\alpha\left|z-z_{1k}\right|\right)-\exp\left(-\alpha\left|z-z_{2k}\right|\right). \end{aligned} \tag{35}$$

For the case when the pencil beam is incident at the center of the cylinder Eq. (35) is simplified to

$$\Phi(\vec{r},\omega) = \frac{1}{2\pi D a'^2}\sum_{n=1}^{\infty}\frac{J_0(s_n\rho)}{\alpha J_1^2(a's_n)}\sum_{k=-\infty}^{\infty}\exp\left(-\alpha\left|z-z_{1k}\right|\right)-\exp\left(-\alpha\left|z-z_{2k}\right|\right). \tag{36}$$

Version B

There is another possibility to solve Eq. (9) for the boundaries given in Eq. (32). By applying the method described in reference [15] the Green's function for a one-dimensional layer is given in the interval $0 \le z < l_z$ as

$$\begin{aligned} G(s_n,z,\omega) &= \frac{\exp(-\alpha\left|z-z_0\right|)-\exp(-\alpha(z+z_0+2z_b))}{2D\alpha}-\frac{\sinh\left[\alpha(z_0+z_b)\right]}{D\alpha} \\ &\quad\times\frac{\sinh\left[\alpha(z+z_b)\right]\exp(-\alpha(l_z+2z_b))}{\sinh\left[\alpha(l_z+2z_b)\right]}\,. \end{aligned} \tag{37}$$

We note that for the evaluation of Eq. (37) no approximation is needed, in contrast to the solutions presented earlier [15]. In general, the solution calculated with Eq. (37) is faster than the solution obtained with Eq. (33), if l_z is small.

Finally, Eq. (37) is inserted in Eq. (20) to obtain the fluence rate for a pencil beam incident at an arbitrary position, in Eq. (21) for a pencil beam incident in the middle of the cylinder top, or in equation Eq. (31) for an incident flat beam.

Solutions in the time domain

Version A

For the derivation of the solution of the fluence rate in the time domain we start with the ordinary differential equation [Eq. (8)]. The boundary conditions given in Eq. (32) are fulfilled by using a finite sine transform:

$$\Phi(\lambda_k) = \int_{z_1}^{z_2}\Phi(z)\sin(\lambda_k(z-z_1))\mathrm{d}z, \quad \lambda_k = k\pi/(z_2-z_1), \quad k=1,2,\ldots, \tag{38}$$

where $z_1 = -z_b$ and $z_2 = l_z + z_b$. By applying Eq. (38) and the following relation

$$\int_{z_1}^{z_2}\frac{\partial^2}{\partial z^2}\Phi(z)\sin(\lambda_k(z-z_1))\mathrm{d}z = \lambda_k[\Phi(z_1)-(-1)^k\Phi(z_2)]-\lambda_k^2\Phi(\lambda_k) \tag{39}$$

#124184 - $15.00 USD Received 12 Feb 2010; revised 7 Apr 2010; accepted 14 Apr 2010; published 21 Apr 2010

we obtain from Eq. (8)

$$\left(s_n^2+\lambda_k^2+\frac{\mu_a}{D}+i\frac{\omega}{Dc}\right)\Phi=\frac{1}{D}J_m(s_n\rho_0)\sin(\lambda_k(z_0+z_b))\cos(m(\phi-\phi_0))\,. \tag{40}$$

Thus, the fluence rate in the frequency domain is given by

$$\Phi(s_n,\phi,m,\lambda_k,\omega)=\frac{cJ_m(s_n\rho_0)\sin(\lambda_k(z_0+z_b))\cos(m(\phi-\phi_0))}{Dc(s_n^2+\lambda_k^2)+\mu_a c+i\omega}\,. \tag{41}$$

The fluence rate in the time domain is obtained from the solutions in the frequency domain using the following Fourier transform

$$\int_{-\infty}^{\infty}\exp(-at)\varepsilon(t)\exp(-i\omega t)dt=\frac{1}{a+i\omega},\quad a>0\,, \tag{42}$$

where $\varepsilon(t)$ describes the Heaviside step function. By employing Eq. (42), Eq. (41) becomes

$$\begin{aligned}\Phi(s_n,\phi,m,\lambda_k,t) &= cJ_m(s_n\rho_0)\sin(\lambda_k(z_0+z_b))\cos(m(\phi-\phi_0))\\ &\quad\times\exp(-\mu_a ct)\exp(-Dc\lambda_k^2 t)\exp(-Dcs_n^2 t),\quad t>0\,.\end{aligned} \tag{43}$$

We use the completeness relation for the sine function to obtain an inversion formula of Eq. (38)

$$\Phi(z)=\frac{2}{z_2-z_1}\sum_{k=1}^{\infty}\Phi(\lambda_k)\sin(\lambda_k(z-z_1))\,. \tag{44}$$

Finally, the inversion formula given in Eq. (20) is used to obtain the time resolved fluence rate in real space

$$\begin{aligned}\Phi(\vec{r},t) &= \frac{2c}{\pi a'^2(l_z+2z_b)}\exp(-\mu_a ct)\sum_{k=1}^{\infty}\exp(-Dc\lambda_k^2 t)\sin(\lambda_k(z_0+z_b))\sin(\lambda_k(z+z_b))\\ &\quad\times\sum_{m=-\infty}^{\infty}\cos(m\varphi)\sum_{n=1}^{\infty}\exp(-Dcs_n^2 t)J_m(s_n\rho_0)J_m(s_n\rho)J_{m+1}^{-2}(a's_n)\,.\end{aligned} \tag{45}$$

For a pencil beam incident onto the center of the cylinder top Eq. (45) is simplified to

$$\begin{aligned}\Phi(\vec{r},t) &= \frac{2c}{\pi a'^2(l_z+2z_b)}\exp(-\mu_a ct)\sum_{k=1}^{\infty}\exp(-Dc\lambda_k^2 t)\sin(\lambda_k(z_0+z_b))\sin(\lambda_k(z+z_b))\\ &\quad\times\sum_{n=1}^{\infty}\exp(-Dcs_n^2 t)J_0(s_n\rho)J_1^{-2}(a's_n)\,.\end{aligned} \tag{46}$$

Version B

We also present a second possibility to solve Eq. (8). Considering again the boundary conditions given in Eq. (32) the series of point sources already applied for version A of the frequency solutions is used, see Eq. (33), where α is now $\alpha=\sqrt{\mu_a/D+s_n^2+i\omega/Dc}$. By employing the Fourier transform

$$\int_{-\infty}^{\infty}\frac{1}{\sqrt{\pi t}}\exp(-at)\exp\left(-\frac{b^2}{4t}\right)\varepsilon(t)\exp(-i\omega t)\mathrm{d}t=\frac{\exp(-|b|\sqrt{a+i\omega})}{\sqrt{a+i\omega}},\quad a>0 \tag{47}$$

#124184 - $15.00 USD Received 12 Feb 2010; revised 7 Apr 2010; accepted 14 Apr 2010; published 21 Apr 2010

the solution for the homogeneous cylinder in the time domain is for an arbitrary incident pencil beam

$$\Phi(\vec{r},t) = \frac{1}{2\pi a'^2}\sqrt{\frac{c}{D\pi t}}\exp(-\mu_a ct)\sum_{k=-\infty}^{\infty}\exp\left(-\frac{(z-z_{1k})^2}{4Dct}\right)-\exp\left(-\frac{(z-z_{2k})^2}{4Dct}\right) \times\sum_{m=-\infty}^{\infty}\cos(m\varphi)\sum_{n=1}^{\infty}\exp(-Dcs_n^2t)J_m(s_n\rho_0)J_m(s_n\rho)J_{m+1}^{-2}(a's_n)\,. \quad (48)$$

For the pencil beam incident at the middle of the cylinder top we get

$$\Phi(\vec{r},t) = \frac{1}{2\pi a'^2}\sqrt{\frac{c}{D\pi t}}\exp(-\mu_a ct)\sum_{k=-\infty}^{\infty}\exp\left(-\frac{(z-z_{1k})^2}{4Dct}\right)-\exp\left(-\frac{(z-z_{2k})^2}{4Dct}\right) \times\sum_{n=1}^{\infty}\exp(-Dcs_n^2t)J_0(s_n\rho)J_1^{-2}(a's_n)\,. \quad (49)$$

2.1.2. Solutions derived via modified Bessel differential equation

In this section we derive the solutions of the homogeneous diffusion equation for an incident pencil beam by solving the modified Bessel differential equation. We start in the frequency domain and, then, give the time domain solution.

The modified Bessel differential equation is obtained by neglecting the z-dependency in Eq. (2)

$$\frac{\partial^2}{\partial\rho^2}\Phi+\frac{1}{\rho}\frac{\partial}{\partial\rho}\Phi+\frac{1}{\rho^2}\frac{\partial^2}{\partial\phi^2}-\alpha^2\Phi=-\frac{1}{D}\delta(\rho-\rho_0)\delta(\phi-\phi_0)\,, \quad (50)$$

where $\alpha=\sqrt{\mu_a/D+i\omega/Dc}$. This differential equation can be solved considering the radial boundary condition $\Phi(\rho=a',\omega)=0$. The solution can be derived by using a formula given in reference [6] as

$$\Phi(\rho,\varphi,\omega) = \frac{1}{2\pi D}\left[K_0(\alpha\sqrt{\rho^2+\rho_0^2-2\rho\rho_0\cos\varphi}) - \sum_{m=-\infty}^{\infty}\cos(m\varphi)\frac{I_m(\alpha\rho_0)K_m(\alpha a')I_m(\alpha\rho)}{I_m(\alpha a')}\right]. \quad (51)$$

I_m and K_m denote the modified Bessel functions of first and second kind of mth order. By setting $\alpha=\sqrt{\mu_a/D+\lambda_k^2+i\omega/(Dc)}$ and multiplying the right side of Eq. (50) with $\sin(\lambda_k(z_0+z_b))$, we obtain the same result as if we had performed a finite sine transform related to the z-coordinate, compare Eq. (38). By applying the inverse transform, see Eq. (44), we get the fluence rate for an arbitrary incident beam position

$$\Phi(\vec{r},\omega) = \frac{1}{4\pi D}\sum_{k=-\infty}^{\infty}\frac{\exp(-\mu_{eff}r_1)}{r_1}-\frac{\exp(-\mu_{eff}r_2)}{r_2}-\frac{1}{\pi D(l_z+2z_b)} \times\sum_{k=1}^{\infty}\sin(\lambda_k(z_0+z_b))\sin(\lambda_k(z+z_b))\sum_{m=-\infty}^{\infty}\cos(m\varphi)\frac{I_m(\alpha\rho_0)K_m(\alpha a')I_m(\alpha\rho)}{I_m(\alpha a')}\,, \quad (52)$$

#124184 - $15.00 USD Received 12 Feb 2010; revised 7 Apr 2010; accepted 14 Apr 2010; published 21 Apr 2010

where

$$\begin{aligned} r_1 &= \sqrt{\rho^2+\rho_0^2-2\rho\rho_0\cos\varphi+(z-z_{1k})^2} \\ r_2 &= \sqrt{\rho^2+\rho_0^2-2\rho\rho_0\cos\varphi+(z-z_{2k})^2} \\ \mu_{eff} &= \sqrt{\mu_a/D+i\omega/Dc}\,. \end{aligned} \tag{53}$$

The transmitted light from the cylinder barrel is found by using the ρ derivative for the modified Bessel functions, see Eq. (22). The result is

$$\begin{aligned} T(\varphi,z,\omega) &= \frac{a-\rho_0\cos\varphi}{4\pi}\sum_{k=-\infty}^{\infty}(\mu_{eff}+1/r_1)\frac{\exp(-\mu_{eff}r_1)}{r_1^2}-(\mu_{eff}+1/r_2)\frac{\exp(-\mu_{eff}r_2)}{r_2^2} \\ &+\frac{1}{\pi(l_z+2z_b)}\sum_{k=1}^{\infty}\sin(\lambda_k(z_0+z_b))\sin(\lambda_k(z+z_b)) \\ &\times\sum_{m=-\infty}^{\infty}\cos(m\varphi)\frac{I_m(\alpha\rho_0)K_m(\alpha a')\left[\alpha I_{m+1}(\alpha\rho)+m/aI_m(\alpha a)\right]}{I_m(\alpha a')}\,. \end{aligned} \tag{54}$$

For a pencil beam incident onto the middle of the cylinder top the fluence rate is

$$\begin{aligned} \Phi(\vec{r},\omega) &= \frac{1}{4\pi D}\sum_{k=-\infty}^{\infty}\frac{\exp(-\mu_{eff}r_1)}{r_1}-\frac{\exp(-\mu_{eff}r_2)}{r_2} \\ &-\frac{1}{\pi D(l_z+2z_b)}\sum_{k=1}^{\infty}\sin(\lambda_k(z_0+z_b))\sin(\lambda_k(z+z_b))\frac{K_0(\alpha a')I_0(\alpha\rho)}{I_0(\alpha a')}\,, \end{aligned} \tag{55}$$

and the transmittance is obtained with

$$\begin{aligned} T(z,\omega) &= \frac{a}{4\pi}\sum_{k=-\infty}^{\infty}(\mu_{eff}+1/r_1)\frac{\exp(-\mu_{eff}r_1)}{r_1^2}-(\mu_{eff}+1/r_2)\frac{\exp(-\mu_{eff}r_2)}{r_2^2} \\ &+\frac{1}{\pi(l_z+2z_b)}\sum_{k=1}^{\infty}\alpha\sin(\lambda_k(z_0+z_b))\sin(\lambda_k(z+z_b))\frac{K_0(\alpha a')I_1(\alpha a)}{I_0(\alpha a')}\,. \end{aligned} \tag{56}$$

For the solution in the time domain, the frequency domain solution, $\Phi(\vec{r},\omega)$, is used and split into real and imaginary parts [17]. Then, the inverse Fourier transform is calculated by using the FFT algorithm.

Alternatively, we used the 'damping' rule of the Laplace transform for separation of that part in Eq. (52) which contains the z-coordinate [18]. The result is

$$\begin{aligned} \Phi(\vec{r},t) &= \frac{1}{4\pi D\sqrt{\pi Dct}}\sum_{k=-\infty}^{\infty}\exp\left(-\frac{(z-z_{1k})^2}{4Dct}\right)-\exp\left(-\frac{(z-z_{2k})^2}{4Dct}\right) \\ &\times\left[\frac{1}{2t}\exp(-\mu_a ct)\exp\left(-\frac{\rho^2-\rho_0^2-2\rho\rho_0\cos\rho}{4Dct}\right)\right. \\ &\left.-\frac{1}{2\pi}\sum_{m=-\infty}^{\infty}\cos(m\varphi)\int_{-\infty}^{\infty}\frac{I_m(\mu_{eff}\rho_0)K_m(\mu_{eff}a')I_m(\mu_{eff}\rho)}{I_m(\mu_{eff}a')}\exp(i\omega t)\mathrm{d}\omega\right]\,, \end{aligned} \tag{57}$$

and the transmittance is obtained with

$$T(\varphi,z,t) = \frac{1}{4\pi\sqrt{\pi Dct}}\sum_{k=-\infty}^{\infty}\exp\left(-\frac{(z-z_{1k})^2}{4Dct}\right)-\exp\left(-\frac{(z-z_{2k})^2}{4Dct}\right)$$

#124184 - $15.00 USD Received 12 Feb 2010; revised 7 Apr 2010; accepted 14 Apr 2010; published 21 Apr 2010

$$\times \left[\frac{a-\rho_0\cos\varphi}{4Dct^2} \exp(-\mu_a ct) \exp\left(-\frac{a^2-\rho_0^2-2a\rho_0\cos\rho}{4Dct} \right) \right.$$
$$\left. + \frac{1}{2\pi} \sum_{m=-\infty}^{\infty} \cos(m\varphi) \int_{-\infty}^{\infty} \frac{I_m(\mu_{eff}\rho_0) K_m(\mu_{eff}a') I'_m(\mu_{eff}a)}{I_m(\mu_{eff}a')} \exp(i\omega t) \mathrm{d}\omega \right] , \tag{58}$$

where $I'_m(\mu_{eff}a) = \partial I_m(\mu_{eff}\rho)/\partial\rho|_{\rho=a} = \mu_{eff} I_{m+1}(\mu_{eff}a) + m/a I_m(\mu_{eff}a)$.

The integral is solved by applying the inverse discrete Fourier transform. The calculations using Eq. (58) are approximately 2 orders of magnitude faster than those calculated without using the 'damping' rule.

2.2. Monte Carlo Simulations

The solutions of the diffusion equation are compared to results obtained by Monte Carlo simulations. The Monte Carlo program we developed is able to handle different geometries. For the simulations presented in this study a cylindrical geometry is employed. The light is incident perpendicular to the cylinder top both as a pencil light beam and as a circular flat beam having a finite radius. The refractive index of the cylinder and the surrounding medium is set to $n_0 = n_1 = 1.0$. The Henyey-Greenstein phase function is used for calculating the scattering angles using an anisotropy factor of $g = 0.8$. 10^7 photons were used in Monte Carlo simulations.

3. Results

In this section we, first, compare the different solutions of the diffusion equation derived in the steady-state, frequency, and time domains among themselves. Then, we compare the derived solutions of the diffusion theory with Monte Carlo simulations.

3.1. Comparison of the different solutions of the diffusion equation

For the first comparison the cylinder is illuminated by a pencil beam. It is incident onto the cylinder barrel perpendicular to the barrel at a depth of $z = 8$mm, see inset of Fig. 2. The steady-state transmittance is calculated around the cylinder barrel at a depth of $z = 10$mm. The height and radius of the cylinder are $l_z = 20$mm and $a = 5$mm, respectively. The reduced scattering coefficient is $\mu'_s = 0.9\mathrm{mm}^{-1}$, whereas the absorption coefficient is varied ($\mu_a = 0.005, 0.01, 0.015\mathrm{mm}^{-1}$). For the calculations shown in Fig. 2 we used Eq. (54) for $\omega = 0$. As expected the transmitted light decreases up to the opposite point relative to the incident beam (at $\phi = \pi$) and the transmittance is smaller for increasing absorption coefficients.

Next, we compare the different solutions of the steady-state diffusion equation for the cylinder shown in Fig. 2. The relative difference of two of the three solutions [(Eqs. (35)–(54)]/[Eq. (35)] is shown in Fig. 3. The relative differences are in the range of 10^{-10}, thus, the agreement is excellent. The relative differences between the two steady-state solutions calculated via the Hankel transform (version A and version B) are even smaller (data not shown).

Subsequently, the solutions in the time domain are compared. Figure 4 shows the time resolved transmittance from a homogeneous cylinder having a radius of $a = 9$mm and a height of $l_z = 12$mm. The cylinder barrel is illuminated at $z_0 = 9$mm and the transmittance is detected at $z = 9$mm on the opposite site of the cylinder ($\phi = \pi$) (black curve) and at the middle of the cylinder bottom (red curve).

#124184 - $15.00 USD Received 12 Feb 2010; revised 7 Apr 2010; accepted 14 Apr 2010; published 21 Apr 2010

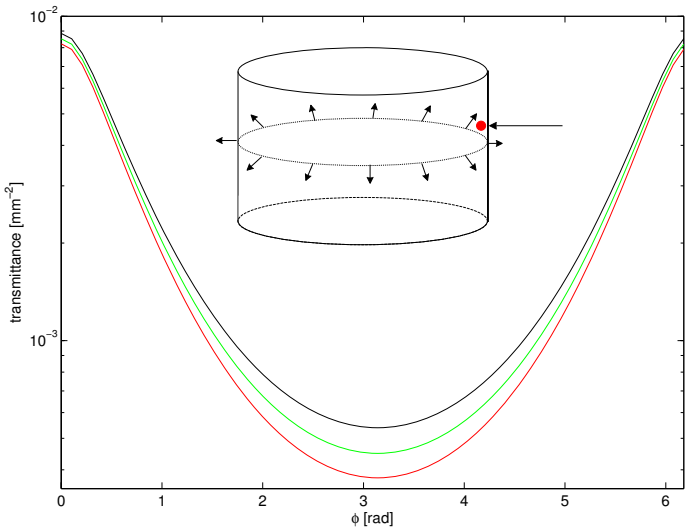

Fig. 2. Steady-state radial transmittance around the cylinder barrel at $z = 10$mm and $\rho = a$. The cylinder is illuminated perpendicular to the cylinder barrel at $z_0 = 8$mm, see inset. The optical parameters are $\mu_s' = 0.9\text{mm}^{-1}$, $\mu_a = 0.005\,(\text{black}), 0.01\,(\text{green}), 0.015\,(\text{red})\text{mm}^{-1}$, $n_0 = 1.0$, and $n_1 = 1.4$. The geometrical data of the cylinder are $a = 5$mm and $l_z = 20$mm.

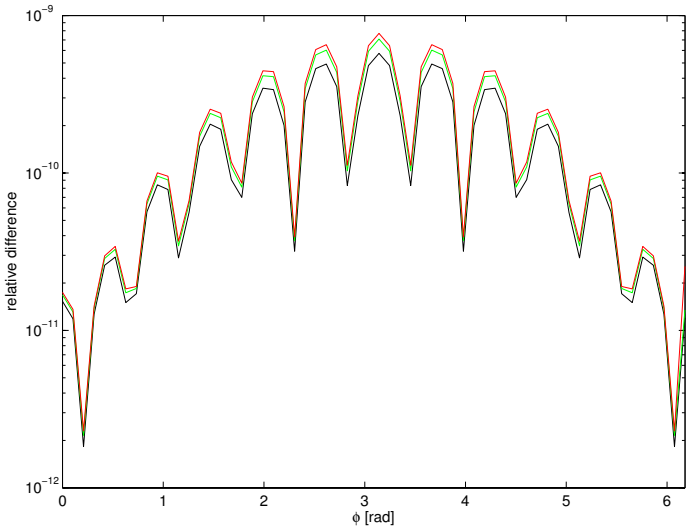

Fig. 3. Relative difference of two steady-state solutions for the cylinder considered in Fig. 2.

#124184 - $15.00 USD Received 12 Feb 2010; revised 7 Apr 2010; accepted 14 Apr 2010; published 21 Apr 2010

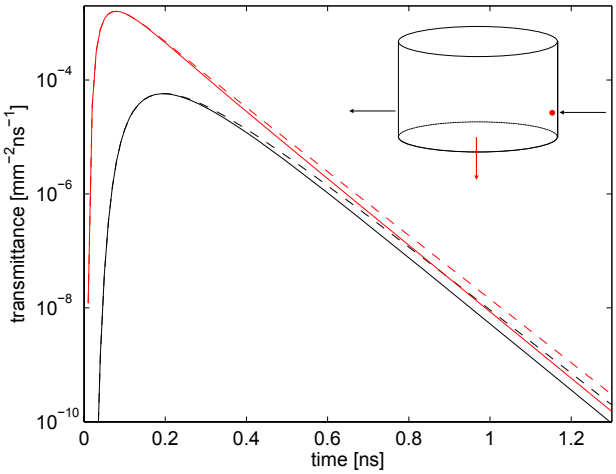

Fig. 4. Time resolved transmittance from a cylinder that is illuminated at the cylinder barrel at $z_0 = 9$mm. The transmittance is detected in z-direction at $z = l_z$, $\rho = 0$mm (red curve) and in radial direction at $z = 9$mm, $\rho = a$ (black curve). The optical and geometrical parameters are $\mu_s' = 0.8\text{mm}^{-1}$, $\mu_a = 0.03\text{mm}^{-1}$, $n_0 = 1.0$, $n_1 = 1.4$, $a = 9$mm, and $l_z = 12$mm. The dashed curves show the transmittance from a homogeneous cube.

Figure 4 shows the results calculated with Eq. (48) (solid curves). The relative difference between the three solutions in the time domain is smaller than 10^{-10} (data not shown). For comparison, in Fig. 4 also the time resolved transmittance from a rectangular parallelepiped is shown for both detection positions (dashed curves) [8]. The lengths of the edges of the parallelepiped in x-, y-, and z-directions are 9mm, 9mm, and 12mm, respectively. As expected, the results diverge for longer times when the detected photons have experienced the region where the two geometries (cylinder and parallelepiped) are different.

For frequency domain measurements an intensity modulated beam, which consists of a continuous and a sinusoidally oscillating part, is incident onto the turbid medium. In the following we consider only the oscillating part. Figure 5 shows the results of the oscillating part ($\omega_0 = 2\pi \cdot 500\text{MHz}$) for a pencil beam that is incident onto the cylinder barrel computed with the solution obtained by solving the modified Bessel differential equation. The light transmitted from the barrel at an angle of $\phi = 3\pi/4$ at the same height is shown. The transmittance is computed for different cylinder radii $a = 5$mm (black curve), $a = 6$mm (green curve), $a = 7$mm (red curve).

In order to compare the solution shown in Fig. 5 to the solution obtained with the hyperbolic functions (version B) in the frequency domain, we calculated the transmittance by using the following time harmonic signal

$$S(\vec{r},t) = \delta(\vec{r} - \vec{r}_0)\cos(\omega_0 t)\ . \tag{59}$$

The transmittance is given by

$$T(\vec{r},t) = \text{Re}\left\{T(\vec{r},\omega = \omega_0)e^{i\omega_0 t}\right\}\ . \tag{60}$$

The disagreement between the two solutions is small. Thus, we give the numerical values

#124184 - $15.00 USD Received 12 Feb 2010; revised 7 Apr 2010; accepted 14 Apr 2010; published 21 Apr 2010

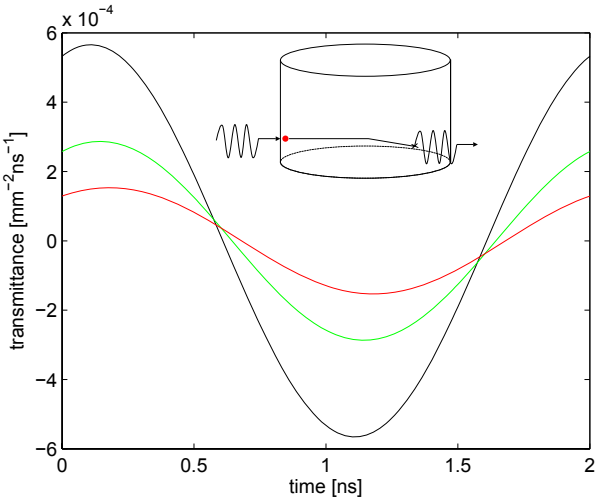

Fig. 5. The transmittance of a sinusoidally oscillating source incident at $z = 12$mm, $\rho = a$ and detected at the same height at $\phi = 3\pi/4$. The optical and geometrical parameters are $\mu_s' = 0.7\text{mm}^{-1}$, $\mu_a = 0.02\text{mm}^{-1}$, $n_0 = 1.0$, $n_1 = 1.4$, $a = 5, 6, 7$mm, $l_z = 22$mm, $z_0 = 11$mm. The modulation frequency is $\omega_0 = 2\pi \cdot 500$MHz.

for the above curve having a radius of $a = 6$mm:

$$T(\vec{r}, \omega_0) = 10^{-4}\text{mm}^{-2} \times \begin{cases} 2.5774906387 - 1.2540621701i \\ 2.5774906366 - 1.2540621700i \end{cases} . \tag{61}$$

The upper complex number is calculated with the solution derived by solving the modified Bessel differential equation and the lower number with the hyperbolic functions. Thus, the relative differences are in the order of 10^{-10}.

3.2. Comparison with Monte Carlo simulations

The solutions of the diffusion equation are, first, compared to Monte Carlo simulations for an incident pencil beam, and, then, for an incident flat beam. Figure 6 and Fig. 7 show the spatially resolved reflectance and transmittance from the cylinder top and bottom, respectively. The radius of the cylinders is $a = 14$mm, whereas the height of the cylinders is $l_z = 5$mm (blue curves) and $l_z = 10$mm (red curves). The optical properties are $\mu_s' = 1.3\text{mm}^{-1}$ and $\mu_a = 0.008\text{mm}^{-1}$.

In general, the results of the Monte Carlo simulations (circles) agree well with those obtained from the diffusion theory (solid curves) both for the spatially resolved reflectance and transmittance. For small distances of the spatially resolved reflectance the differences are larger due to the well-known break down of the diffusion theory. At large distances the influence of the border on the light propagation can be seen causing a stronger decrease in the remitted and transmitted intensities. As expected, the increase of the height of the cylinder results in an increase of the remitted light especially at large distances from the source, whereas the transmittance is decreased at small distances and increased at large distances.

Figure 8 shows the spatially resolved reflectance from a homogeneous cylinder that is illuminated in the middle of the top side by a flat beam having radii of $\rho_w = 0$mm (blue curve), $\rho_w = 5$mm (green curve), and $\rho_w = 10$mm (red curve). We note that the beam

#124184 - $15.00 USD Received 12 Feb 2010; revised 7 Apr 2010; accepted 14 Apr 2010; published 21 Apr 2010

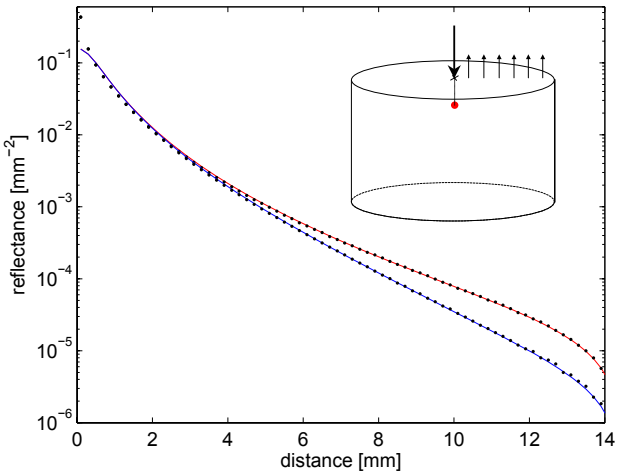

Fig. 6. Comparison of the spatially resolved reflectance calculated with the solution of the diffusion equation and with the Monte Carlo method for a turbid cylinder illuminated with a pencil beam in the middle of the cylinder top. The optical and geometrical parameters of the cylinders are $\mu_s' = 1.3\text{mm}^{-1}$, $\mu_a = 0.008\text{mm}^{-1}$, $a = 14\text{mm}$, $n_1 = n_0 = 1.0$, $l_z = 5$ and 10mm.

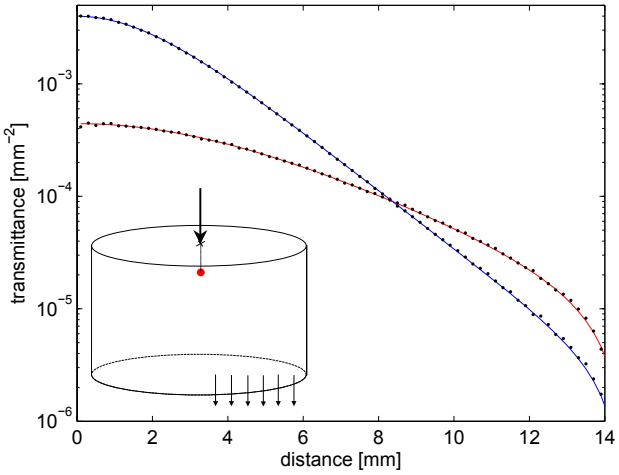

Fig. 7. Comparison of the spatially resolved transmittance calculated with the solution of the diffusion equation and with Monte Carlo simulations for a turbid cylinder illuminated with a pencil beam in the middle of the cylinder top. The optical and geometrical parameters of the cylinders are $\mu_s' = 1.3\text{mm}^{-1}$, $\mu_a = 0.008\text{mm}^{-1}$, $a = 14\text{mm}$, $n_1 = n_0 = 1.0$, $l_z = 5$ and 10mm.

#124184 - $15.00 USD Received 12 Feb 2010; revised 7 Apr 2010; accepted 14 Apr 2010; published 21 Apr 2010

with $\rho_w = 0$mm corresponds to a pencil beam. The optical properties of the cylinder are $\mu_s' = 1.2\text{mm}^{-1}$ and $\mu_a = 0.01\text{mm}^{-1}$. The radius and height are $a = 20$mm and $l_z = 5$mm, respectively.

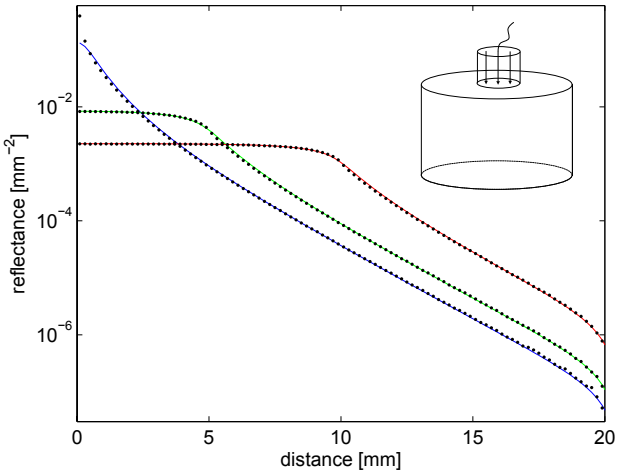

Fig. 8. Spatially resolved reflectance from a homogeneous cylinder that is illuminated by a flat beam with $\rho_w = 0, 5, 10$mm. The optical and geometrical parameters are $\mu_s' = 1.2\text{mm}^{-1}$, $\mu_a = 0.01\text{mm}^{-1}$, $a = 20$mm, $l_z = 5$mm, and $n_1 = n_0 = 1.0$.

In general, Fig. 8 shows good agreement between diffusion theory and Monte Carlo simulations. Interestingly, the break down of the diffusion equation at small distances can only be seen for $\rho_w = 0$mm. For large beam diameters the agreement is even good for small distances from the source.

4. Discussion

Solutions of the diffusion equation for a homogeneous cylinder were derived in the steady-state, frequency, and time domains. Comparison of the reflectance and transmittance calculated with these solutions showed excellent agreement among themselves in each domain. The speed for calculation of the solutions, however, are different. In the time domain we found for the general case of a beam incident at an arbitrary position that the solution obtained via solving the modified Bessel differential equation is about hundred times faster than the other two solutions. For example, the time needed for obtaining the time resolved transmittance using Eq. (58) is in the order of 10ms on a state-to-the-art computer programmed in Pascal (Delphi).

The derived solutions permit the calculation of the fluence rate for a pencil beam that is incident at an arbitrary position onto the surface of the cylinder. In addition, we derived the solutions for a circular flat beam incident onto the plane surfaces of the turbid cylinder for all three domains.

The solutions of the diffusion equation were compared to Monte Carlo simulations. Good agreement was found as expected from results calculated for turbid media having other geometries. Interestingly, quite a good agreement was obtained for the spatially resolved reflectance at small distances from the center of the incident circular beam having finite beam diameters, although it is expected that diffusion theory breaks down in this case. Probably, the distance dependent errors of the solution of the diffusion

#124184 - $15.00 USD Received 12 Feb 2010; revised 7 Apr 2010; accepted 14 Apr 2010; published 21 Apr 2010

equation for an incident pencil beam (at small distances diffusion theory gives larger and at very small distances smaller values than Monte Carlo simulations) cancel out for finite beam diameters, compare Fig. 8.

Acknowledgement

We acknowledge the support by the European Union (nEUROPt, grant agreement no. 201076).

#124184 - $15.00 USD Received 12 Feb 2010; revised 7 Apr 2010; accepted 14 Apr 2010; published 21 Apr 2010